PERGAMON

Journal of Structural Geology 22 (2000) 1511–1522

JOURNAL OF STRUCTURAL GEOLOGY

www.elsevier.nl/locate/jstrugeo

Numerical modelling of single-layer folding: clarification of an issue regarding the possible effect of computer codes and the influence of initial irregularities

Y. Zhang[a,*], N.S. Mancktelow[b], B.E. Hobbs[a], A. Ord[a], H.B. Mühlhaus[a]

[a]*Australian Geodynamics Cooperative Research Centre, CSIRO Exploration & Mining, Nedlands, WA 6009, Australia*
[b]*Geologisches Institut, ETH-Zentrum, CH-8092 Zürich, Switzerland*

Received 10 January 2000; accepted 18 May 2000

Abstract

The influence of initial perturbation geometry and material properties on final fold geometry has been investigated using finite-difference (FLAC) and finite-element (MARC) numerical models. Previous studies using these two different codes reported very different folding behaviour although the material properties, boundary conditions and initial perturbation geometries were similar. The current results establish that the discrepancy was not due to the different computer codes but due to the different strain rates employed in the two previous studies (i.e. 10^{-6} s^{-1} in the FLAC models and 10^{-14} s^{-1} in the MARC models). As a result, different parts of the elasto-viscous rheological field were being investigated. For the same material properties, strain rate and boundary conditions, the present results using the two different codes are consistent. A transition in folding behaviour, from a situation where the geometry of initial perturbation determines final fold shape to a situation where material properties control the final geometry, is produced using both models. This transition takes place with increasing strain rate, decreasing elastic moduli or increasing viscosity (reflecting in each case the increasing influence of the elastic component in the Maxwell elasto-viscous rheology). The transition described here is mechanically feasible but is associated with very high stresses in the competent layer (on the order of GPa), which is improbable under natural conditions.

1. Introduction

Folds are some of the most commonly observed deformation structures in nature and the mechanics of their development has been extensively studied over the last half-century (e.g. Biot, 1959, 1961; Ramberg, 1960; Chapple, 1968; Sherwin and Chapple, 1968; Hudleston, 1973; Cobbold, 1975; Treagus, 1973; Fletcher, 1974, 1977, 1979; Smith, 1977, 1979, Johnson and Fletcher, 1994). A comprehensive review can be found in Price and Cosgrove (1990). From this large body of work it is clear that the shape and wavelength of folds potentially provide one of the few sources of direct information on rock rheology under natural conditions. However, what is less well established is how effectively this rheological control may be masked by the shape and distribution of initial perturbations in the layer surface. Analogue scale-model experiments indicate that the influence may be quite strong, especially for isolated initial irregularities of finite amplitude (e.g. Cobbold, 1975; Abbassi and Mancktelow, 1990, 1992). However, numerical modelling of single-layer folding in elasto-viscous materials has so far produced contradictory results. Zhang et al. (1996), using a finite-difference code (FLAC) observed that a clearly defined dominant wavelength was rapidly established that is largely independent of the initial perturbation's position and shape. In contrast, Mancktelow (1999), using a finite-element code (MARC), obtained results similar to the analogue models, i.e. with a dominant influence of the initial perturbation geometry. This

* Corresponding author.

0191-8141/00/$ - see front matter
PII: S0191-8141(00)00063-8

apparent contradiction is puzzling since the material properties, boundary conditions and initial perturbation geometry in the studies were directly comparable. At the same time, there is no obvious reason why the different codes, both of which have been extensively tested, should give different results.

In this comparative study, the discrepancy is explained. The strain rate (10^{-6} s^{-1}) used by Zhang et al. (1996) was significantly greater than the rate (10^{-14} s^{-1}) adopted by Mancktelow (1999). For the Maxwell elasto-viscous model rheology employed in both these earlier studies (and again here, for direct comparison), the relative contribution of elasticity to the overall rheological behaviour was correspondingly more important in the high strain rate experiments and single-layer folding was being investigated in distinctly different rheological regimes. In this study, models with the same initial geometry, material properties and boundary conditions were deformed at identical rates using the two different codes (i.e. FLAC and MARC). The finite-element and finite-difference codes return the same results, except for one remaining discrepancy related to edge effects. The important issue of what actually controls fold shapes is also explored here by investigating a wide range of the strain rate–viscosity–elastic moduli–competence contrast space in the models.

2. Description of the methods and models

2.1. Finite difference FLAC models

One of the two computer codes employed in this study is the finite-difference code, FLAC (Fast Lagrangian Analysis of Continua, Cundall and Board 1988; see also www.itascacg.com). This code uses an approach whereby the discretized equations are solved by a dynamic relaxation scheme. FLAC incorporates a very efficient strategy for the handling of volumetric constraints and the relaxation technique is also robust in modelling localization. The code has been successfully used to simulate a number of problems in structural geology (e.g. Hobbs et al., 1990; Ord, 1990; McKinnon and Barra, 1998).

2.2. Finite element MARC models

The other code employed is the commercial finite-element-modelling package MARC–Mentat (see www.marc.com). MARC represents the finite-element program itself, whereas Mentat is the graphic user interface for model generation and post-processing. The program is specifically written for considering non-linear problems, such as arise due to a combination of elasto-viscous behaviour and large strain. Details of the code and methods are summarized in Mancktelow (1999).

2.3. Model geometry and boundary conditions

The geometry of the model consists of a central competent layer, embedded in a less competent matrix, and initially seeded with either a series of periodic small perturbations or a single isolated perturbation. The layer thickness is 2 units, the model length 198 units and the width 128 units, identical to the two previous studies. For a symmetric isolated initial perturbation at the centre of the layer, only one half of the model needs to be calculated if asymmetric modes do not occur in response to the symmetrical perturbation. Test results for half and full finite-element models are identical (Mancktelow 1999) and consequently only one half was actually calculated in the finite-element models of symmetrical isolated perturbations presented here. Progressive shortening parallel to the layer was achieved by velocity boundary conditions applied to the edges of the model. In the FLAC models this velocity was kept constant (a constant 'engineering strain rate', $de/dt = [1/l_o][dl/dt]$, where e is elongation, t is time and l_o is the initial layer length), whereas in the MARC models the velocity was varied in inverse proportion to the model length (a constant 'logarithmic strain rate', $d\varepsilon/dt = [1/l][dl/dt]$, where l is the current layer length). Any differences in the results due to this slight discrepancy in boundary conditions should only be developed at large total shortening and are not at all apparent in the comparative models presented here.

In all cases, the x-velocity of the convergent sides was prescribed by the above relationships and these sides were thus maintained perfectly planar. The y-velocity of nodes along the same sides was generally unconstrained, with the exception of the midpoint in some models as outlined below. In the case of MARC models with isolated perturbations, where the reflection symmetry was utilized and only one half of the model considered, the x-velocity of the reflection plane was set to zero and the y-velocity unconstrained. To check the influence of boundary conditions, two sets of finite-element models were performed. In the first set (corresponding to those of Mancktelow, 1999), the upper and lower sides of the model were left free. An additional fixed y-velocity node was then required to eliminate any potential for rigid body translation. For isolated perturbations and cosine-form periodic perturbations (inflection point at boundary) the mid-point of the convergent side(s) was given a y-velocity of zero. For sine-form periodic perturbations (hinge point at boundary), it was the central point of the whole model (which then lies on an inflection point of the initial perturbation) for which the y-velocity was set to zero. In the second set of experiments, the y-velocity of the

upper and lower sides was constrained to be equal but opposite in sign, so that the sides are forced to remain planar. In this case, no additional y-velocity constraints are necessary and the zero y-velocity nodes at the mid-point or centre of the models, as described for the first set, are no longer introduced. For the model dimensions considered here, the two sets of boundary conditions produce identical results, as also noted by Mancktelow (1999).

In the original study of Zhang et al. (1996) and in most FLAC models presented here, a combination of both sets of boundary constraints was employed, with both the y-velocity of the mid-point on the converging sides set to zero and the retreating upper and lower sides maintained straight with equal and opposite y-velocity. In this comparative study, FLAC and MARC models were run with the full range of boundary conditions outlined above. It was found that, for the same imposed conditions, the two codes always produced similar results. However, as discussed further below, when the upper and lower plates are maintained straight, there are clear differences in the final model geometries for the two cases when the mid-point of the converging sides is constrained or not. This boundary condition effect is independent of the code employed but does explain some specific differences in the results of the original publications.

2.4. Material properties

A Maxwell elasto-viscous model for the material rheology is adopted here for consistency with the studies of Mancktelow (1999) and Zhang et al. (1996). This constitutive model is equivalent to a combination of a compressible linear elastic element (spring) and an incompressible Newtonian viscous element (dashpot) in series (see Jaeger and Cook, 1979, p. 315; Ranalli 1987, p. 86). Since perfectly elastic behaviour is instantaneous but viscous resistance is time dependent, it follows that faster strain rates promote more elastic behaviour in the system.

An important material parameter in these models is the *competence contrast* (R) between the layer and the matrix. For a Maxwell elasto-viscous material, R is defined here as the ratio of both viscosity and Young's modulus between the layer (l) and the matrix (m), that is, $R=\eta_l/\eta_m=E_l/E_m$, where η is the viscosity and E is Young's modulus. For a constant Poisson's ratio (the value 0.25 is used throughout, see Table 1), this becomes $R=\eta_l/\eta_m=K_l/K_m=G_l/G_m$, where K and G are the bulk and shear moduli. This follows the approach of the earlier paper of Zhang et al. (1996) rather than Mancktelow (1999), where ratios in elastic moduli were always $=10$ and usually only 1 or 2. The material properties of the models are summarised in Table 1 and will be related to each model in the description below.

This definition of R has its limitations. Although ratios in the effective viscosity of different rocks under natural conditions could reach very high values, perhaps exceeding four orders of magnitude (e.g. Carter and Tsenn, 1987), the maximum ratio in Young's moduli is only on the order of 10 (e.g. Turcotte and Schubert, 1982). However, the purpose here is to model a similar contribution of viscosity and Young's modulus towards competence contrast. It is important to emphasise that the present contribution represents a quite restricted, qualitative exploration of the folding behaviour of Maxwell materials within a restricted subset of the relevant parameter space. To simplify the problem, we have focussed on that part of the parameter space characterised by equal elasticity and viscosity ratios of the competent layer and of the embedding material, for different bulk strain rates. In fact, a complete characterisation of the parameter space requires the explicit consideration of the internal relaxation times of the plate and of the embedding material as well. In doing so, an even richer array of buckling behaviour is revealed in which more than one wavelength is amplified. For instance, Mühlhaus et al. (1998) have shown that there exist dramatically different folding behaviours (involving the development of multiple dominant wavelengths) depending on the values of the relaxation times of the competent layer and of the embedding medium, and on the amplification rates of buckling instabilities. The complete spectrum of such behaviour for the buckling of Maxwell

Table 1
Summary of the material properties of the models. R is competence contrast, E is Young's modulus (Pa) and η is viscosity (Pa s); Poisson's ratio is 0.25 in all the models, and l denotes layer and m denotes matrix

	R = 20		R = 50		R = 100		R = 200	
Group	η_l/η_m	E_l/E_m	η_l/η_m	E_l/E_m	η_l/η_m	E_l/E_m	η_l/η_m	E_l/E_m
1	2e20/1e19	7e10/3.5e9	5e20/1e19	17.5e10/3.5e9	1e21/1e19	3.5e11/3.5e9	2e21/1e19	7e11/3.5e9
2	2e23/1e22	3.5e10/1.75e9	2e23/4e21	3.5e10/7e8	2e23/2e21	3.5e10/3.5e8	2e23/1e21	3.5e10/1.75e8
3					1e22/1e20	3.5e10/3.5e8		
4					1e23/1e21	3.5e10/3.5e8		

materials needs to be considered in a future, more extensive study.

3. FLAC finite-difference model results

3.1. Folding related to initial periodic perturbations

The initial, small periodic geometrical perturbations imposed on the layer in the present FLAC models are identical to those used by Zhang et al. (1996, fig. 1)) and Mancktelow, 1999. These comprise 16 full waveforms, each with an initial wavelength of six-times layer thickness and with an initial amplitude 1/20 of the layer thickness. This wavelength is smaller than the theoretical dominant wavelength for purely viscous materials (10.3 times layer thickness for $R = 20$; see Fletcher, 1974, 1977; Mancktelow, 1999, fig. 5a). Models were considered with $R = 20$, 50, 100 and 200 with various strain rates and constitutive parameters.

The first group of models uses the group 1 material properties specified in Table 1. The properties and boundary conditions are identical to those used by Zhang et al. (1996). Fig. 1 gives the final fold geometries of the models with a bulk shortening of 22–30%, and bulk strain rates of 10^{-14} s^{-1}, 10^{-12} s^{-1} and 10^{-10} s^{-1}, respectively.

For the lowest strain rate (10^{-14} s^{-1}), the final fold shapes of the four models with different R are clearly different from those obtained by Zhang et al. (1996, fig. 2a) for a much higher strain rate (10^{-6} s^{-1}), but are similar to those reported by Mancktelow (1999, fig. 2) for the same strain rate of 10^{-14} s^{-1}. Both the initial geometrical waveforms and their wavelength are retained throughout the deformation. This implies that hinge points do not migrate relative to material particles, as already pointed out by Mancktelow (1999), and that the fold wavelength is entirely controlled by the introduced perturbation. In other words, the Biot dominant wavelength, as a function of layer thickness and competence contrast, is not generated under these conditions.

The amplitude of folds for these models is still quite low at 30% bulk shortening. Our analyses show that, at 30% bulk shortening stages, layer-parallel shortening accommodates about 94, 89, 87 and 85% of bulk shortening in these models with $R = 20$, 50, 100 and 200, respectively, only a relatively small amount of bulk shortening being accommodated by dynamic buckling. As a result of this, layer length and thickness decreases and increases linearly, respectively, with increasing shortening. These observations indicate that the dynamic fold growth rate is very small and that homogeneous shortening is dominating these models, consistent with theory for simpler, incompressible viscous materials (e.g. Biot, 1961; Fletcher, 1974, 1977; Smith, 1975) and the earlier finite-element models of elasto-viscous materials (Mancktelow, 1999, Fig. 5b).

Increasing the strain rate has the effects of increasing dynamic fold growth rate and decreasing homogenous

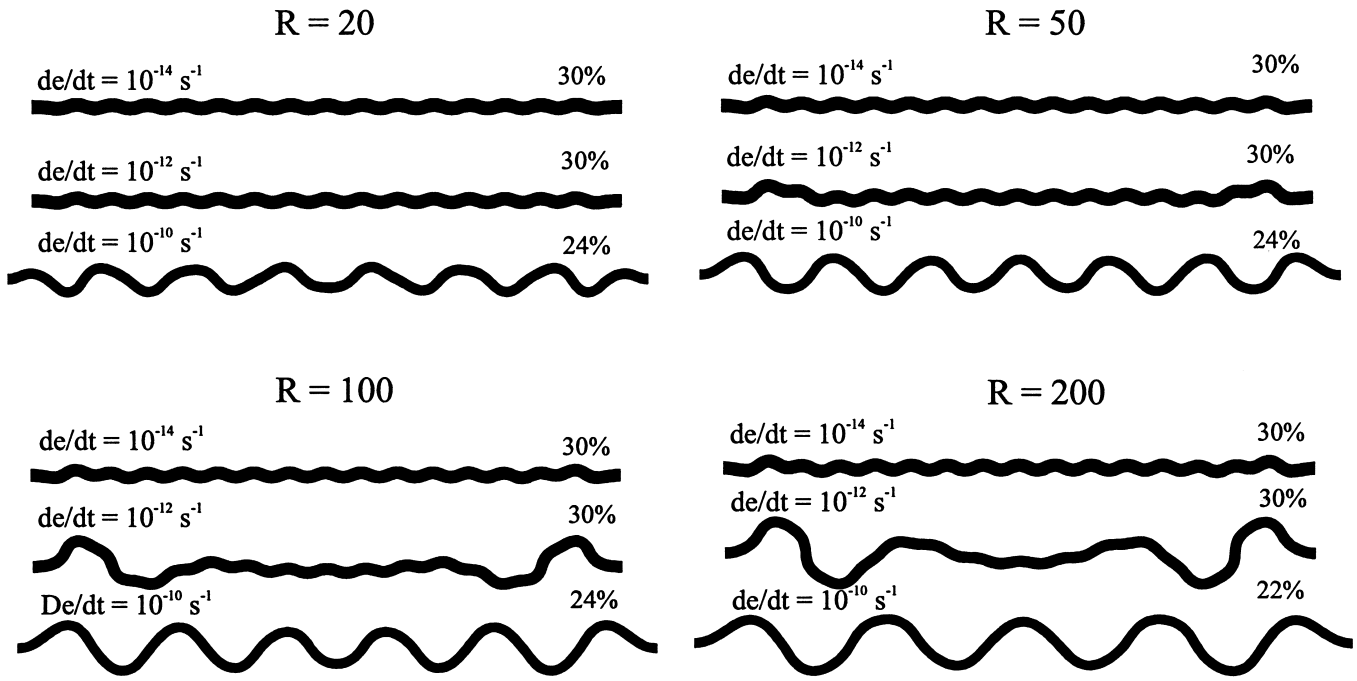

Fig. 1. Fold development in a single layer containing an initial periodic geometric perturbation, for models with group 1 properties as listed in Table 1 and with various strain rates (de/dt) and competence contrasts (R); FLAC models.

bulk shortening (Fig. 1). At a strain rate of 10^{-12} s^{-1}, the results for higher competence contrasts (R = 50, 100 and 200) show clear departures from the smaller strain-rate situation where homogeneous shortening is dominating; now wavelengths related to the competence contrast start to develop. Increasing the strain rate to 10^{-10} s^{-1} results in a further increase of fold growth rates (Fig. 1). Dynamic fold amplification starts to dominate and accommodate most of the shortening, with new wavelengths (close to the Biot wavelengths) fully developed and outpacing the growth of the initial shorter wavelength. This is convergent towards the results obtained by Zhang et al. (1996) for a much higher strain rate. Such dynamic fold growth (wavelength selection) does require the migration of hinge points of initial small perturbations but this occurs at a stage when limb dips are still small. Fold growth in this process shows an 'explosive' development, as widely described by previous workers (e.g. Biot 1961, Ramsay 1967, Ramberg 1964).

The next group of models (Fig. 2) explores the effects of increasing viscosity and decreasing elastic moduli (Table 1, group 2) for the same initial geometry and with the strain rate fixed at 10^{-14} s^{-1}. This represents a more explicit way to investigate the effect of enhanced elastic behaviour on folding. The results (Fig. 2) confirm that such a change in constitutive parameters has a similar effect to increasing strain rate. Fold development now is dominated by dynamic amplification even at the low strain rate of 10^{-14} s^{-1}, leading to the formation of new wavelengths that are again close to the Biot wavelength for the relevant competence contrast and layer thickness. Note that

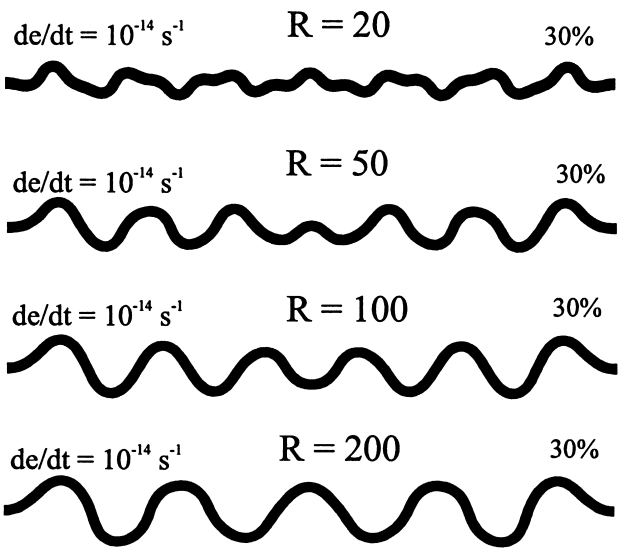

Fig. 2. Final fold geometries for models with the group 2 properties of Table 1 (increased viscosity and decreased elastic moduli), with $de/dt = 10^{-14}$ s^{-1} and various values of R; FLAC models.

fold amplification is weaker at low competence contrast (R = 20) and the fold shape at 30% shortening clearly bears the marks of the initial small perturbations.

To explore further the influence of the wavelength of initial perturbations, we have performed another group of experiments for R = 50, in which the same material properties as the first group (Table 1, group 1) are used but with a larger initial wavelength, close to the relevant Biot wavelength (Fig. 3). At a low strain rate of 10^{-14} s^{-1} (Fig. 3a), fold growth rate remains small until about 20% bulk shortening. Fold growth is basically passive and bulk deformation is mainly accommodated by homogenous shortening up to this point, but then dynamic fold growth intensifies by 30% bulk shortening. During the entire folding process, the hinge points of initial perturbations remain fixed at the same material locations. This is similar to the situation for a smaller initial wavelength (see Fig. 1, for models with a strain rate of 10^{-14} s^{-1}). However, the overall fold growth rate and final fold amplitude are obviously greater, due to a favourable initial wavelength (Fig. 3a). For the same initial geometry, increasing the strain rate to 10^{-10} s^{-1} (Fig. 3b) again has the effect of enhancing dynamic folding growth. Much larger fold amplitude has been achieved by 20% shortening, with layer parallel shortening reduced significantly.

It should be mentioned that in the present FLAC models and the models presented in Zhang et al. (1996), the initial perturbation geometry is such that an inflection point of the initial waveform train falls on the model boundaries. This may be considered equivalent to placing an even smaller geometrical perturbation at the ends of the layer. Mancktelow (1999) raised the concern that this initial geometry may introduce edge effects and additional wavelength components and therefore be responsible for the reported folding transition behaviour. We have tested the models by modifying the model size slightly so that hinge points fall on the model edge; the initial geometry remains the same for much of the model. The models produced exactly the same results as those shown in Fig. 1; strain rate and material mechanical properties are the only controlling factors here. As discussed below, this remains the one important difference between the FLAC and finite-element MARC models presented here.

3.2. Folding related to initial single isolated perturbations

The single layer situation with an initial isolated perturbation has also been simulated here to investigate fold propagation in the layer. The three types of single perturbation employed by Zhang et al. (1996), termed

perturbations A, B and C, respectively, are used here. They are generated using an equation $y(x) = a\cos(\pi x/b)$ so that perturbations A, B and C have an initial amplitude of 1.4 units and initial widths of 18, 38 and 80 units (9, 19 and 40 times layer thickness), respectively. For an easy comparison with the study of Mancktelow (1999), his perfect bell-shaped C-type single perturbation (Abbassi and Mancktelow 1992) is also modelled here, and termed perturbation D.

Fig. 4 shows the results of a group of models which incorporate the group 1 material properties in Table 1 but only examine two competence contrasts (R = 20 and 100). From this summary figure, it is clear that the amplification of the initial isolated perturbations and fold propagation in the layer is different for different strain rates. At 10^{-14} s^{-1}, the amplification of the initial isolated perturbation is weak in all the models, there is no fold hinge migration and, at least up to 30% shortening, there is no significant fold waveform propagation along the layer (Fig. 4). The final geometry is largely controlled by the initial shape of the four types of initial perturbation, combined with large layer-parallel shortening. Competence contrast seems only to affect the final amplitudes of the folds. These features are consistent with those reported by Mancktelow (1999, fig 10) for the same strain rate. This is particularly clear for perturbation D, which is identical to Mancktelow's bell-shaped C-type perturbation.

At a strain rate of 10^{-12} s^{-1}, all the models display larger final fold amplitudes (Fig. 4), reflecting higher growth rates. Some fold waveform propagation is also observed in the models with R = 100. With an increase in the strain rate to 10^{-10} s^{-1}, all the models show waveform propagation along the layer on both sides of the initial isolated perturbation, leading to the development of fold trains with the dominant wavelength. Note that the evolution of C-type initial perturbations is particularly interesting (Fig. 4). These perturbations split into folds of smaller wavelength because the initial wavelength of perturbation C is much greater than the Biot dominant wavelength for the relevant competence contrast and layer thickness. These results converge towards the result of Zhang et al. (1996) for a higher strain rate.

The last two models examine changes induced by increasing viscosity and decreasing elastic moduli (i.e. enhanced elasticity), with the strain rate fixed at 10^{-14} s^{-1}; only perturbation B with R = 100 is simulated. The first model incorporates the group 3 properties of Table 1. The results (Fig. 5a) show that as a result of the change in constitutive properties, fold waveform propagation becomes visible at 20% bulk shortening and is enhanced further at 30% shortening (compare with Fig. 4). The second model uses an even higher viscosity (Table 1, group 4). Now fold waveform propagation (Fig. 5b) becomes clearly visible at 10% shortening, and by 30% shortening, fold propagation has led to the development of a fold train with the dominant wavelength.

4. MARC finite-element model results

4.1. Folding related to initial periodic perturbations

For the same initial perturbation geometries, material properties and boundary conditions, the MARC finite-element code produce results that are effectively identical to those obtained with the FLAC finite-difference code (e.g. compare Fig. 2d and Fig. 6a). As is

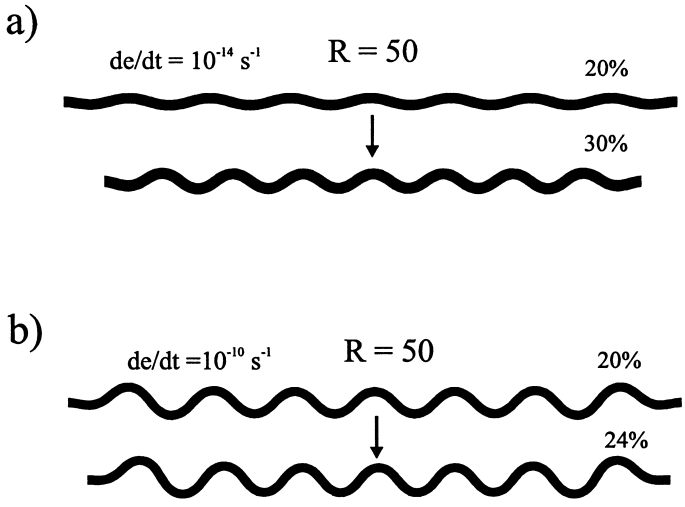

Fig. 3. Final fold geometries for models with a larger initial perturbation wavelength (equal to the dominant wavelength for R = 50, calculated using the equation of Fletcher 1977 for viscous materials); FLAC models. Group 1 properties of Table 1 for R = 50 are used with strain rates of a) 10^{-14} s^{-1} and b) 10^{-10} s^{-1}.

now clear, the original apparent difference only reflects the different strain-rates employed, and therefore the transition to strongly elastic behaviour, as discussed in detail below.

However, one significant difference in the results does remain with regard to the influence of model boundaries on fold geometry. As discussed in Mancktelow (1999), placing the planar model boundaries at an inflection point of the wavetrain causes important boundary effects (e.g. Fig. 1 for strain rates of 10^{-12} s^{-1}; see also Mancktelow, 1999, Fig. 1), which in turn introduces new spectral components, of small but finite amplitude, into the system. With increasingly elastic behaviour, the dynamic growth rate and rate of sideways propagation along the layer (e.g. see Fig. 4) of these components is so high compared to the input perturbation that they eventually dominate the overall structure and produce a final 'dominant wavelength' shape independent of the initial periodic wavetrain (Fig. 6a). This does not occur for finite-element models with hinge points at the boundaries (Fig. 6c). The initial perturbation wavelength in this example is much smaller than the fastest growing dominant wavelength and the growth rate is correspondingly low, with most of the imposed bulk shortening accommodated by layer-parallel shortening. This system is highly metastable, since any spectral component closer to the dominant wavelength would grow faster and in an ex-

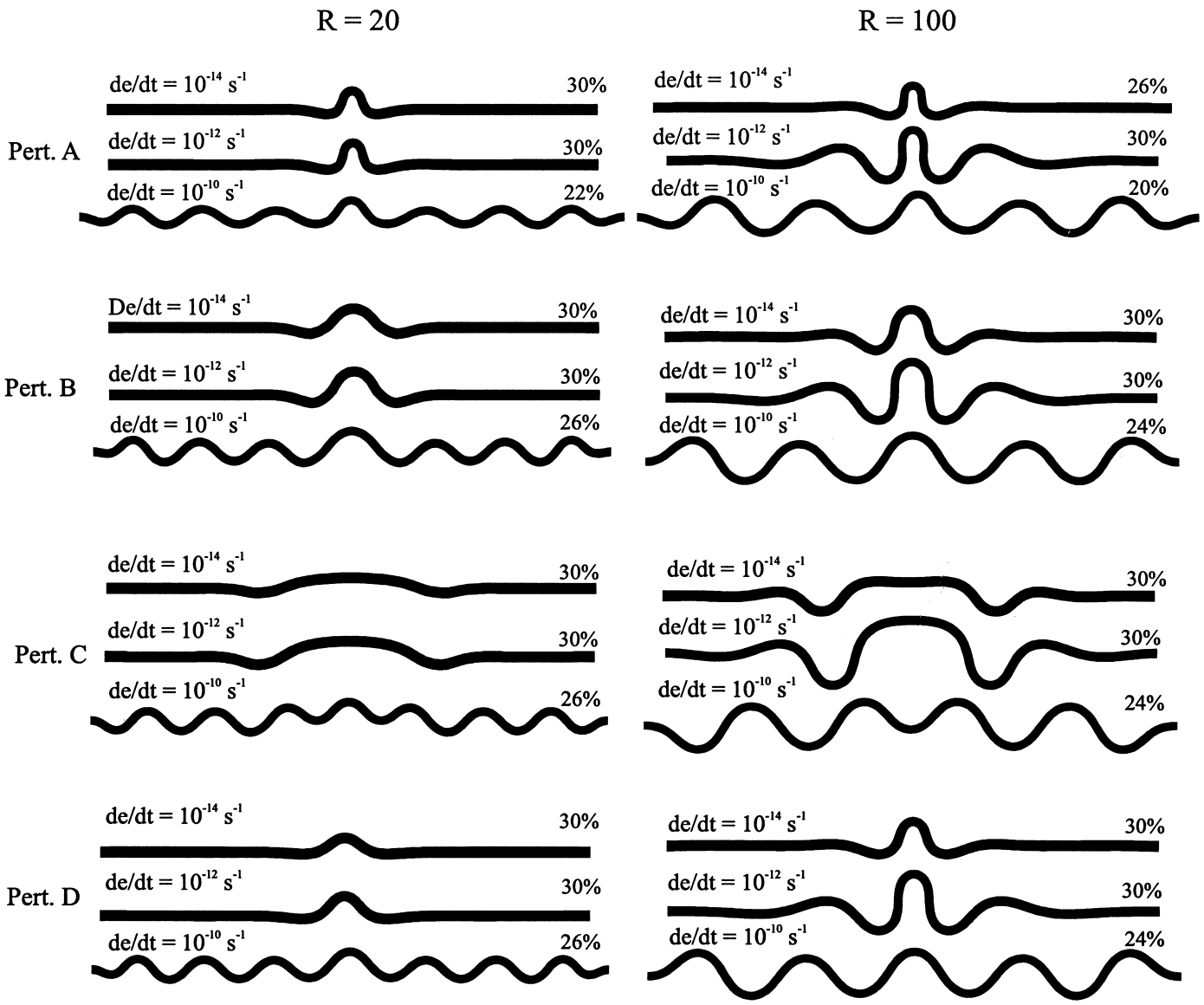

Fig. 4. Fold development in a single layer with an initial isolated geometric perturbation; FLAC models. Final fold geometries are shown for the models with Pert. A, B, C (cosine forms) and D (bell-shaped form) for different strain rates (de/dt). Group 1 properties of Table 1 for $R = 20$ and 100 are used.

ponential manner. This effect is exacerbated as the maximum growth grate is increased with increasingly elastic behaviour. The slightest divergence from a perfect sinusoidal perturbation would indeed result in the rapid development of a wavetrain closer to the 'dominant wavelength'. Since there are always small differences in numerical truncation scheme between different numerical modelling codes, it is quite possible that the FLAC models do bifurcate in this specific case to still develop the dominant wavelength, while the MARC models do not. It is also true that the explicit scheme used in FLAC generally promotes the continuation of the initial perturbed mode of deformation of each model, while MARC uses an implicit solver, so that singularities (corresponding to secondary bifurcation) may affect the performance of the algorithm if the deformation is indeed metastable.

In nature, perfectly sinusoidal initial irregularities never occur. However, it is still important to establish if individual Fourier components can be analysed independently, at least for low fold amplitudes. This approach allows growth rate curves to be determined, for example, by Fourier transformation of folds developed from initial isolated bell-shaped perturbations and analysis of the growth of the individual spectral components (e.g. Mancktelow and Abbassi, 1992). It is also a necessary justification for considering only a half wavelength 'unit cell' of a perfectly periodic form, as done in many previous numerical studies of folding (e.g. Dieterich and Carter, 1969).

One minor difference in the final geometry of the FLAC and MARC results in the original publications is directly related to the different boundary constraints applied. In the models of Zhang et al. (1996), both the velocity of the upper and lower divergent sides and the midpoints of the convergent sides were constrained, whereas in the finite-element models of Mancktelow (1999) either the midpoints or the divergent sides were constrained, but never both. The double constraint condition forces the ends of the layer to remain on the midline (e.g. Figs. 1–5 and Fig. 6a), whereas for the less constrained condition, a fully periodic geometry develops in which a fold hinge occurs at the boundary (Fig. 6b, Figs. 7 and 8). This is because the hinge axial plane represents a natural symmetry plane in the final fold structure and the model can be considered as a segment of an infinite wavetrain.

4.2. Folding related to initial single isolated perturbations

Again, it is readily established that the original differences in the results of the earlier studies were not due to the different codes but a result of the difference in strain rates employed. Minor discrepancy could arise occur due to the different shapes of the isolated perturbations used in the two original studies. Mancktelow and Abbassi (1992) and Mancktelow (1999) followed Biot et al. (1961) in using a bell-shaped perturbation following the equation $y = b/[1 + (x/a)^2]$,

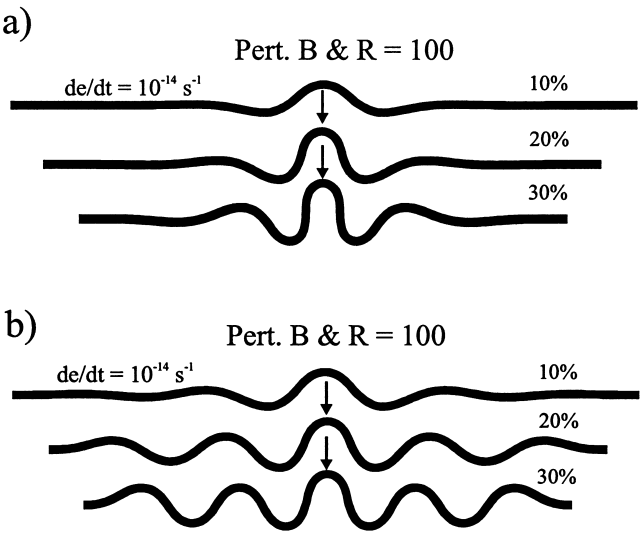

Fig. 5. Evolution of folding for models developed from Pert. B with $R = 100$ but with increased viscosity and decreased elastic moduli in comparison to Fig. 4; FLAC models. (a) Model incorporating the group 3 properties of Table 1. (b) Model incorporating the group 4 properties of the Table 1.

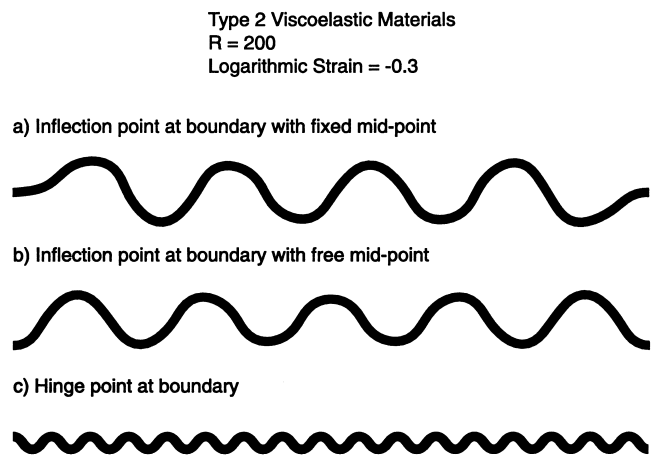

Fig. 6. Finite-element models showing the influence of edge effects on fold shapes for a bulk logarithmic strain of –0.3 (26% shortening), group 2 material properties (Table 1) and $R = 200$, for a constant natural strain rate $d\varepsilon/dt = 10^{-14}$ s^{-1}. The model parameters are the same as in Fig. 2; MARC models. (a) The two side boundaries of the model correspond to inflection points in the wavetrain, with the midpoint of the layer fixed at the convergent boundaries and the divergent upper and lower model boundaries constrained to be planar, the same as in Fig. 2. (b) No constraint was placed on the midpoint of the layer at the convergent boundaries. (c) The wavetrain was shifted a quarter wavelength so that the convergent side boundaries now correspond to hinge points. Other conditions are the same as in (b).

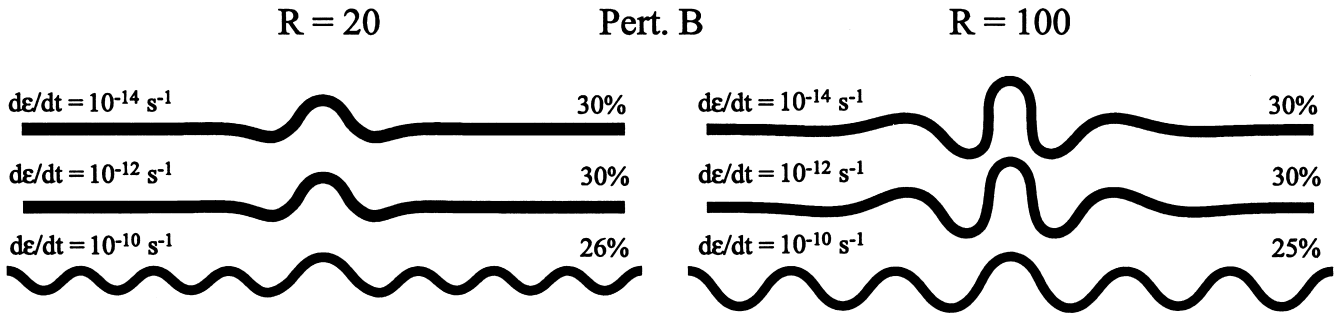

Fig. 7. Finite-element models of folding developed from an initial isolated perturbation, with parameters identical to Pert. B of Fig. 4; MARC models.

where b is the amplitude and a determines the width and therefore the spectral distribution. Zhang et al. (1996) used a smoothed cosine form, as defined above. Here both forms are used to establish a one-to-one correspondence.

Comparison of the Pert. B model from Fig. 4 with the finite-element models of Fig. 7 and the Pert. D model of Fig. 4 with the corresponding Pert. C model of figure 10 in Mancktelow (1999) for a strain-rate of 10^{-14} s^{-1} clearly establishes that essentially the same results are obtained. This is particularly clearly demonstrated by the identical results for the strain rate of 10^{-12} s^{-1} (Figs. 4 and 7).

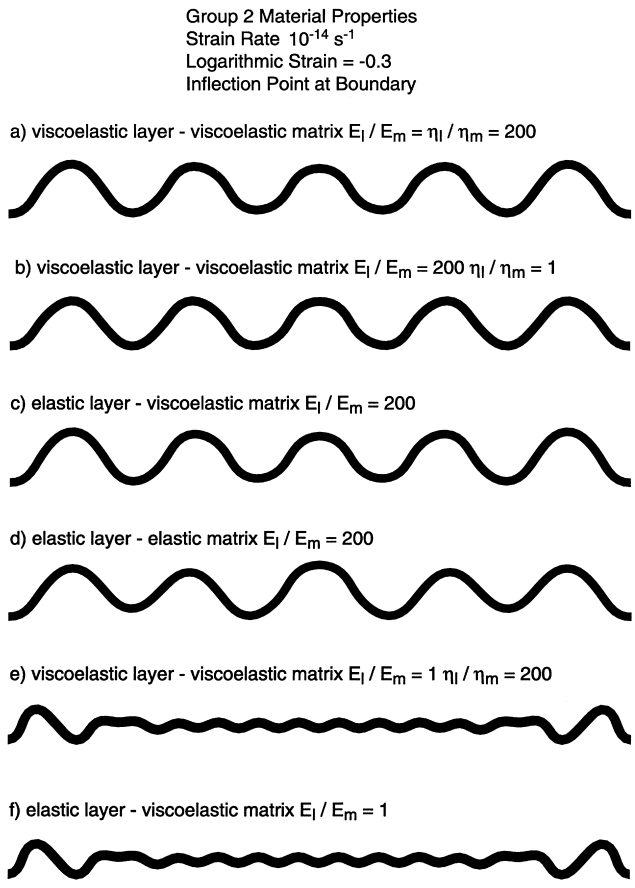

Fig. 8. Analysis of the influence of the different possible ratios in viscosity and Young's moduli on fold shape at a bulk shortening of –0.3 logarithmic strain (26% shortening); MARC models. Values of either 200:1 or 1:1 are employed. In (e) and (f), the behaviour of a perfectly elastic layer in an elasto-viscous matrix is also investigated, and in (d) the case of an elastic layer in an elastic matrix. The magnitudes of the parameters correspond to the group 2 materials properties with $R = 200$ in Table 1. For ratios between layer and matrix of 1:1, the value for the layer in Table 1 was used for both layer and matrix.

5. Discussion

The transition in folding behaviour reported in Zhang et al. (1996) and discussed in Mancktelow (1999) is again produced in this study. This transition reflects a change of folding behaviour from a situation where the geometry of initial perturbation determines final fold shape (no hinge migration) to a situation where the geometry of final folds is controlled by material mechanical properties, largely irrespective of initial geometry (strong hinge migration). As is now unequivocally established, this transition is a direct result of the increasing influence of the elastic component in the Maxwell elasto-viscous rheology employed, either due to increasing strain rate or changing material properties. The important question is whether this transition is to be expected under natural conditions.

Fig. 8 presents the results of a sensitivity analysis (using MARC) of the influence of the different possible combinations of elastic and viscous parameters for the group 2 materials (with $R = 200$) as used in Fig. 2. The results demonstrate that it is the ratio in elastic moduli that ultimately determines the periodic fold shape developed for the group 2 properties (and implicitly the models of Fig. 1 with strain rate of 10^{-10} s^{-1}). The final shape for $R = 200$ in Fig. 2 is closely approximated by a purely elastic model (Fig. 8d). Including viscous behaviour allows the stresses to relax

during folding, so that stress levels are not as high as in the purely elastic case and the folds maintain their shape during stress relaxation (e.g. if the boundaries are held fixed at the end of the experiment). However, the elastic behaviour is dominant in actually establishing the fold shape. This is also clear from Fig. 9a, where it can be seen that most strain is elastic at the time the periodic fold train is established. From Fig. 9b, it can be seen that large compressive (inner arc) and tensional (outer arc) stresses are associated with the development of such folds (in this case corresponding to Figs. 2 and 8a, with $R = 200$). Differential and mean stresses are on the order of GPa, magnitudes increasing toward the inner and outer arcs of the fold hinges (in other words, the traverse of Fig. 9b does not represent maximal values). Indeed, this figure is only an illustrative example. All the fold trains developed above the transition to periodic forms in Fig. 4 (i.e. with strain rate 10^{-10} s^{-1}) involve high stresses on the order of many GPa. It is questionable if such stress values could ever be attained in natural folds, since failure, especially on the extending outer fold arcs, would limit the ultimate strength of the rock. Biot (1961) brought exactly the same argument to suggest that the influence of elastic behaviour on rock folding would only be limited. For the transition to occur in nature, a model must be capable of simulating the behaviour while maintaining stresses at realistic levels, and further work is required to test this possibility by exploring a wider material property-strain rate space or other geologically-relevant constitutive laws, especially those that involve yielding before such high stresses arise.

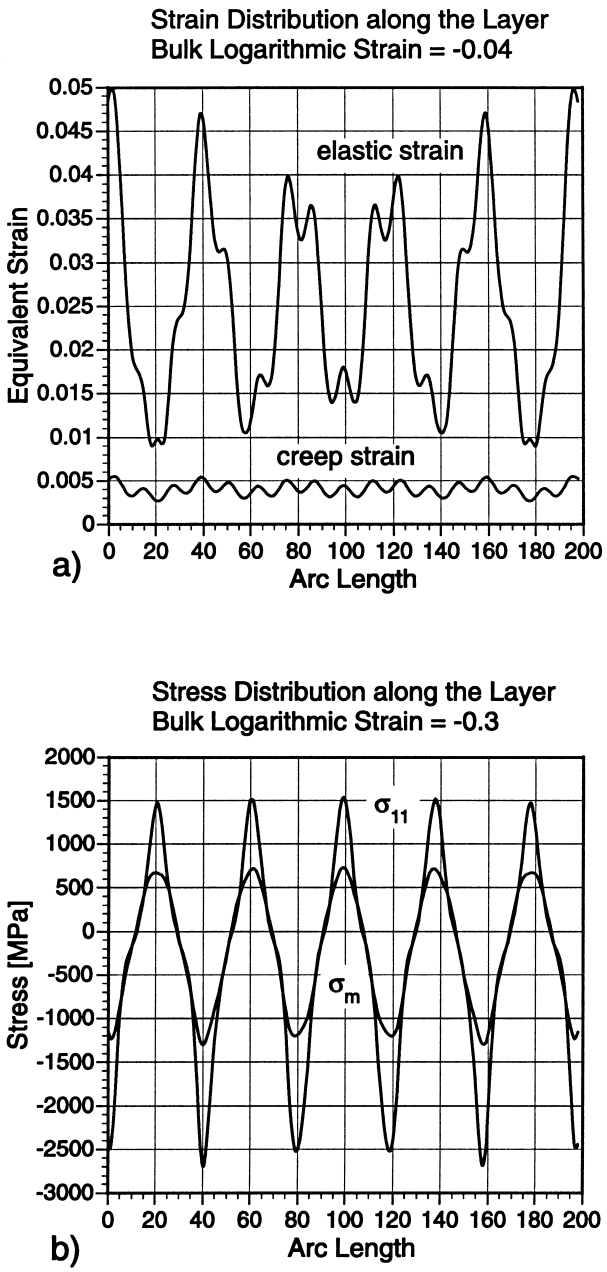

Fig. 9. Plots of strain and stress versus initial cumulative arc length along the layer for the example of Fig. 6a (MARC models), which corresponds to the FLAC model with $R = 200$ in Fig. 2. The plots follow a line initially three quarters of the distance between the centre of the layer and the upper edge. (a) Equivalent (or 'effective') elastic and creep strain components (e.g. Ranalli, 1987, p. 76) at logarithmic strain = –0.04, when establishment of the dominant wavelength different from the initial perturbation is well established. Note that elastic strains predominate. (b) Normal stress σ_{11} and mean stress σ_m distribution along the same line, for bulk logarithmic strain = –0.3 (the same as in Fig. 6). Note that compressive stress is negative and that magnitudes are up to 2.5 GPa.

The transition in the controlling fold mechanism for elasto-viscous materials has recently also been analysed by Schmalholz and Podladchikov, 1999. They propose that the transition to more elastically influenced folding behaviour is not only determined by the stress in the layer but also by the ratio between layer and matrix viscosity. They define the controlling factor as the ratio of the viscous dominant wavelength to the elastic dominant wavelength for the particular material properties. Since the smaller of these two wavelengths in an elasto-viscous material will always amplify faster, there will be a crossover in dominant buckling mechanism when this ratio is unity. The definition involves both the viscosity ratio (to power 1/3) and the ratio of the layer-parallel stress to the elastic shear modulus (to power 1/2). For constant viscosity ratio, it follows that increasing strain rate or deceasing magnitude of the elastic modulus should lead to a transition to folding dominated by elastic behaviour, as demonstrated here. However, for constant strain rate and elastic modulus in the layer, an increase in viscosity ratio can have the same effect. This may be discernible in the modelling results presented here (e.g. Fig. 1) and could be important in natural examples with a large layer–matrix viscosity contrast. However, a direct comparison is not possible, since Schmalholz and Podladchikov, 1999 consider an elasto-viscous layer in a viscous matrix,

whereas in the current models all materials are elasto-viscous and, for direct comparison with Zhang et al. (1996), the ratio in the viscosities and the elastic moduli between layer and matrix are always the same.

6. Conclusions

Numerical models of single-layer folds obtained using the finite difference code (FLAC) are consistent with those using the finite element code (MARC) for the same material properties, strain rate and boundary conditions. The differences in the results reported by Zhang et al. (1996) and Mancktelow (1999) were not due to the different computer codes used in the two studies. The explanation lies in the different strain rates employed in the two studies, namely 10^{-6} s^{-1} by Zhang et al. (1996) and 10^{-14} s^{-1} by Mancktelow (1999), which meant that quite different parts of the elasto-viscous rheological field were being investigated. This finding removes any uncertainty about possible major effects due to different computer codes on modelling results.

The transition in folding behaviour reflecting the discrepancy in results between the two previous studies can be reproduced with both codes either by increasing the strain rate or decreasing the elastic moduli, equivalent to increasing the elastic component to the material response. Increasingly elastic behaviour results in a faster growth rate and the 'explosive' development of a strongly periodic wavetrain, as is well seen in the experiments with an initial isolated perturbation. This folding process involves strong hinge migration.

A sensitivity analysis of material parameters between layer and matrix for models above the transition in folding behaviour establishes that the major control on the geometry of the periodic forms is the ratio in elastic moduli. The geometry developed is the same as would be obtained for an elastic layer in an elastic matrix. This result reflects the original definition of R in Zhang et al. (1996), namely as the constant ratio in both viscosity and Young's moduli between layer and matrix. At high values of R and strain rate, it is the strong contrast in elastic properties that determines the fold geometry above the transition. This is mechanically feasible but not necessarily realistic for natural rocks because of the associated very high stresses developed in the competent layer (on the order of GPa). Such stresses would be difficult to attain in natural rocks due to the limiting effects of rupture, particularly on the outer arc of folds.

One discrepancy between the modelling results still remains with regard to perfectly periodic initial perturbations. This difference is entirely related to whether the lateral model boundaries are at an initial hinge or inflection point. For both cases, FLAC models show a transition with increasingly elastic behaviour to folding at near dominant wavelength, with associated hinge migration at low amplitudes. In contrast, MARC models only show a comparable transition with hinge migration when the boundaries are at an initial inflection point. In the case of a perfectly sinusoidal initial perturbation with hinges at the model boundaries, there is no hinge migration and the final fold wavelength is entirely controlled by the initial perturbation. This discrepancy has important implications for designing other numerical models. In the case of perfectly periodic initial perturbations, the symmetry of the system is such that in principle only a single quarter wavelength needs to be modelled if hinge migration is not possible. On the contrary, if hinge migration at low amplitudes is possible, only initial perturbations with initial wavelength close to the theoretical dominant wavelength may be analysed in this way.

Acknowledgements

Reviews by John Watkinson and Peter Cobbold are gratefully acknowledged. We would also like to thank Ray Fletcher for his comments on an earlier brevia version of this paper. This paper is published with the permission of the Director of the AGCRC.

References

Abbassi, M.R., Mancktelow, N.S., 1990. The effect of initial perturbation shape and symmetry on fold development. Journal of Structural Geology 12, 273–282.

Abbassi, M.R., Mancktelow, N.S., 1992. Single layer buckle folding in non-linear materials—I. Experimental study of fold development from an isolated initial perturbation. Journal of Structural Geology 14, 85–104.

Biot, M.A., 1959. On the instability of folding deformation of a layered viscoelastic medium in compression. Journal of Applied Mechanics 26, 393–400.

Biot, M.A., 1961. Theory of folding of stratified viscoelastic media and its implications in tectonics and orogenesis. Geological Society of America Bulletin 72, 1595–1620.

Biot, M.A., Odé, H., Roever, W.L., 1961. Experimental verification of the theory of folding of stratified viscoelatic media. Geological Society of America Bulletin 72, 1621–1632.

Carter, N.L, Tsenn, M.C., 1987. Flow properties of continental lithosphere. Tectonophysics 136, 27–63.

Chapple, W.M., 1968. A mathematic theory of finite-amplitude rock-folding. Geological Society of America Bulletin 79, 47–68.

Cobbold, P.R., 1975. Fold propagation in single embedded layers. Tectonophysics 27, 333–351.

Cundall, P.A., Board, M., 1988. A microcomputer program for modelling large-strain plasticity problems. In: Swoboda, G. (Ed.), Proceedings of the Sixth International Conference on Numerical methods in Geomechanics. Numerical Methods in Geomechanics, 6, pp. 2101–2108.

Dieterich, J.H., Carter, N.L., 1969. Stress history of folding. American Journal of Science 267, 129–154.

Fletcher, R.C., 1974. Wavelength selection in the folding of a single

layer with power-law rheology. American Journal of Science 274, 1029–1043.
Fletcher, R.C., 1977. Folding of a single viscous layer: exact infinitesimal-amplitude solution. Tectonophysics 39, 593–606.
Fletcher, R.C., 1979. The shape of single-layer folds at small but finite amplitude. Tectonophysics 60, 77–87.
Hobbs, B.E., Mühlhaus, H.-B., Ord, A., 1990. Instability, softening and localisation of deformation. In: Knipe, R.J., Rutter, E.H. (Eds.), Deformation Mechanisms, Rheology and Tectonics. Geological Society of London Special Publication 54, pp. 143–165.
Hudleston, P.J., 1973. An analysis of 'single-layer' folds developed experimentally in viscous media. Tectonophysics 16, 189–214.
Jaeger, J.C., Cook, N.G.W., 1979. Fundamentals of Rock Mechanics, 3rd ed. Chapman and Hall, London.
Johnson, A.M., Fletcher, R.C., 1994. Folding of Viscous Layers. Columbia University Press, New York.
Mancktelow, N.S., 1999. Finite-element modelling of single-layer folding in elasto-viscous materials: the effect of initial perturbation geometry. Journal of Structural Geology 21, 161–177.
Mancktelow, N.S., Abbassi, M.R., 1992. Single layer buckle folding in non-linear materials—II. Comparison between theory and experiment. Journal of Structural Geology 14, 105–120.
McKinnon, S.D., Barra, V.G., 1998. Fracture initiation, growth and effect field: a numerical investigation. Journal of Structural Geology 20, 1673–1689.
Mühlhaus, H.B., Sakaguchi, H., Hobbs, B.E., 1998. Evolution of three-dimensional folds for a non-Newtonian plate in a viscous medium. Proceedings of the Royal Society of London A454, 1–23.
Ord, A., 1990. Mechanical controls on dilatant shear zones. In: Knipe, R.J., Rutter, E.H. (Eds.), Deformation Mechanisms, Rheology and Tectonics. Geological Society of London Special Publication 54, pp. 183–192.
Price, N.J., Cosgrove, J.W., 1990. Analysis of Geological Structures. Cambridge University Press, Cambridge.
Ramberg, H., 1960. Relationship between length of arc and thickness of ptygmatically folded veins. American Journal of Science 258, 36–46.
Ramberg, H., 1964. Selective buckling of composite layers with contrasted rheological properties, a theory for simultaneous formation of several orders of folds. Tectonophysics 1, 307–341.
Ramsay, J.G., 1967. Folding and Fracturing of Rocks. McGraw-Hill, New York.
Ranalli, G., 1987. Rheology of the Earth. Allen & Unwin, London.
Schmalholz, S.M., Podladchikov, Y., 1999. Buckling versus folding: importance of viscoelasticity. Geophysical Research Letters 26, 2641–2644.
Sherwin, J.A., Chapple, W.M., 1968. Wavelengths of single layer folds: a comparison between theory and observation. American Journal of Science 266, 167–179.
Smith, R.B., 1975. Unified theory of the onset of folding, boudinage and mullion structure. Geological Society of America Bulletin 86, 1601–1609.
Smith, R.B., 1977. Formation of folds, boudinage and mullions in non-Newtonian materials. Geological Society of America Bulletin 88, 312–320.
Smith, R.B., 1979. The folding of a strongly non-Newtonian layer. American Journal of Science 279, 272–287.
Treagus, S.H., 1973. Buckling stability of a viscous single-layer system oblique to the principal compression. Tectonophysics 19, 271–289.
Turcotte, D.L., Schubert, G., 1982. Geodynamics: Applications of Continuum Physics to Geological Problems. Wiley, New York.
Zhang, Y., Hobbs, B.E., Ord, A., Mühlhaus, H.-B., 1996. Computer simulation of single layer buckling. Journal of Structural Geology 18, 643–655.